

# Rapid Computation of Optimally Safe Tension Distributions for Parallel Cable-Driven Robots

Per Henrik Borgstrom, Brett L. Jordan, Gaurav S. Sukhatme, *Senior Member, IEEE*,  
Maxim A. Batalin, *Member, IEEE*, and William J. Kaiser, *Senior Member, IEEE*

**Abstract**—In this paper, we present a novel linear-program formulation that yields “optimally safe” (OS) tension distributions in parallel cable-driven robots by the introduction of a slack variable. The slack variable also enables explicit computation of a near-optimal, feasible starting point. This, in turn, enables rapid computation of the OS tension distributions. The formulation also contains a parameter that can be used to steer cable tensions toward desired regions of operation. We present static results from two simulated robotic systems that demonstrate the ability of our formulation to avoid tension limits. Simulated execution of highly dynamic trajectories on both systems demonstrates rapid-computation abilities. Furthermore, we present experimental results from a real robotic system that further validate the importance of safe tension distributions.

**Index Terms**—Cable tension distributions, parallel cable-driven robots, parallel robots, redundant robots.

## I. INTRODUCTION

PARALLEL cable-driven robots consist of computer-driven actuators that enable controlled release of cables that act in parallel on an end-effector. Such systems possess several advantages over rigid-link parallel manipulators. Due to the low mass of cables as compared with rigid arms, they are capable of highly dynamic motion. Furthermore, such cable-driven systems can potentially span large workspaces. However, the inability of cables to exert positive, pushing forces complicates the analysis. For example, the feasible workspace of parallel cable-driven platforms is severely impacted. Bosscher *et al.* [1] consider the wrench-feasible workspace (WFW) by defining it as the workspace within which a particular set of wrenches can be applied by the end-effector. Gouttefarde and Gosselin [2] and Stump and Kumar [3] consider the wrench-closure workspace (WCW), which is defined as the space within which the platform can exert any wrench.

Manuscript received January 21, 2009; revised June 9, 2009. First published October 30, 2009; current version published December 8, 2009. This paper was recommended for publication by Associate Editor F. Thomas and Editor G. Oriolo upon evaluation of the reviewers' comments. This work was supported by the U.S. National Science Foundation under Grant ECCS-0725441 and Grant ANI-0331481.

P. H. Borgstrom, B. L. Jordan, M. A. Batalin, and W. J. Kaiser are with the University of California, Los Angeles, CA 90095 USA (e-mail: henrik202@hotmail.com; bjordan5@gmail.com; maxim@cens.ucla.edu; kaiser@ee.ucla.edu).

G. S. Sukhatme is with the University of Southern California, Los Angeles, CA 90089-0781 USA (e-mail: gaurav@usc.edu).

This paper has supplementary downloadable multimedia material available at <http://ieeexplore.ieee.org> provided by the author.

Color versions of one or more of the figures in this paper are available online at <http://ieeexplore.ieee.org>.

Digital Object Identifier 10.1109/TRO.2009.2032957

The inability of cables to exert pushing forces also significantly impacts motion control of parallel cable-driven robots. Oh and Agrawal [4] design a controller that guarantees positive tensions and implement it on a four-cable-driven planar platform. Fang *et al.* [5] use proportion–differential (PD) compensation to control the seven-cable-driven 6-degrees-of-freedom (DOF) SEilGEtriebene Stewart-Plattformen in Theorie und Anwendung (SEGESTA) platform. Furthermore, Kino *et al.* [6] propose a robust PD control method with adaptive compensation, wherein an external sensor (camera) is used to eliminate positioning errors due to errors in actuator placement and cable-length measurement. Other work in the design and control of cable-driven robots includes the Wirepuller-Arm-driven Redundant Parallel (WARP) [7] and FASt Load CONveyance (FALCON) [8] systems.

There has been a lot of prior work in kinematic, static, and dynamic analysis of parallel cable-driven robotic systems. Roberts *et al.* [9] present necessary and sufficient conditions for static equilibrium and derive conditions to completely restrain the robot. The conditions hinge on the existence of a positive right null vector of the structure matrix. A necessary condition for this is that the number of cables, i.e.,  $m$ , exceeds the number of DOFs, i.e.,  $n$ . Redundant cables may also be required to increase the workspace volume or otherwise improve the performance. A manipulator, wherein  $m = n + 1$ , is called *completely restrained*, while, if  $m > n + 1$ , it is called *redundantly restrained*. We define  $r = m - n$  to be the *degree of actuation redundancy*. For completely or redundantly restrained manipulators, the null space of the structure matrix is nonempty, and there may exist an infinite number of valid tension distributions. Thus, optimization routines must be executed to select optimal tension distributions.

While force optimization for redundant rigid-link manipulators can often be performed by unbounded-optimization methods, tension-distribution computations for parallel cable-driven systems are subject to lower limits on cable tension. The resulting bounded-optimization problems generally require iterative solution methods, which suffer from unpredictable worst-case complexity and perform poorly under real-time computation requirements. A discussion of these issues is presented in [10].

There exists some work to determine one-norm minimal tension distributions for redundantly actuated cable-driven robots. Fang *et al.* [5] derive analytical expressions for optimal tension distributions in a completely constrained 6-DOF robot. Their method reduces the computation to a one-variable linear program (LP) with the sum of all tensions used as the objective

function. The optimization is then solved by exhaustively checking all extreme points. This method does not extend to increased degrees of actuation redundancy. Borgstrom *et al.* [11] present a highly efficient LP solver for a four-cable-driven, 2-DOF robot. Other previous work [12]–[14] has also suggested the use of LP methods to compute one-norm minimal tensions distributions.

There are several drawbacks associated with one-norm minimal-tension-distribution methods. First, iterative LP solvers used to solve such optimizations require feasible starting points. In general, finding these starting points is nontrivial, and a special phase 1 LP must be solved before the original problem is solved by a phase 2 solver. While previous work [10] suggests the use of tension distribution that was computed during the previous servoloop as a starting point, there is no guarantee that this distribution is feasible, and a phase 1 routine must still be executed. Also, because the optimal point in an LP is always located at an extreme point of the feasible polyhedron, tension distributions found through one-norm minimal formulations are prone to discontinuities, as the optimal operating point may jump from one extreme point to another between successive computations [15], [16]. The resulting step changes in tension may excite high-frequency oscillations in cables and otherwise degrade the performance.

Other works have suggested the use of bounded quadratic programming (QP) methods in computing two-norm optimal tension distributions for parallel cable-driven systems. Borgstrom *et al.* [15] consider a cable-array crane and provide efficient solutions for minimum-norm tension distributions, which are shown to yield improved energy efficiency and continuous cable tensions. However, their methods do not extend to redundantly restrained systems. Hassan and Khajepour [17] use Dykstra's alternating-projection algorithm to find the minimum-norm tension distribution for a pair of simulated robotic systems. This is an iterative convex-optimization method that requires a large number of iterations to converge.

Both the LP and QP methods discussed previously suffer from another significant drawback: Because they aim to minimize cable tensions in the one-norm or two-norm sense, respectively, resulting tensions frequently reside on the lower tension limit. This results in low robot stiffness, and leaves the system prone to slack conditions [16]. To address this issue, Mikelsons *et al.* [16] propose a noniterative method to find "safe" tension distributions that avoid tension limits. Furthermore, they prove that the resulting tension distributions are continuous. However, the proposed method suffers from poor-execution time for even moderately complex systems, as the computational intensity increases combinatorially with the number of cables.

In this paper, we present a novel LP formulation that yields "optimally safe" (OS) tension distributions by means of the introduction of a slack variable  $S$ . The introduction of  $S$  also enables direct computation of a near-optimal, feasible starting point. This, in turn, enables highly efficient computation of OS tension distributions. The formulation also contains a parameter  $\alpha$  that can be used to steer cable tensions toward desired regions of operation.

The remainder of this paper is structured as follows. In Section II, we provide a brief background on LP. In Section III,

we describe previous work in safe tensions and detail our novel LP formulation and the methods used to efficiently compute OS tension distributions. In Section IV, we introduce two cable-driven robotic systems for which we provide static tension distribution results that demonstrate the effect of our formulation on tension distributions. In Section V, we demonstrate the computational efficiency of our solution method by providing results from simulated execution of highly dynamic trajectories. In Section VI, we provide experimental results gathered from a real robotic system, i.e., networked infomechanical system for planar translation (NIMS-PL) [11], and in Section VII, we conclude our paper and describe future research thrusts.

## II. LINEAR PROGRAMMING

Before describing our method of computing optimal tension distributions, we begin by providing a brief introduction to the LP theory. A more complete review of LP theory is available in, for example, [18]. An LP is one in which the objective is to minimize a linear function subject to linear equality and inequality constraints. Because an equality constraint can be represented as two inequality constraints, it is sufficient to consider only inequalities. Thus, a typical LP problem might be

$$\begin{aligned} \bar{p} &= \min_{\mathbf{c}} \boldsymbol{\lambda}^T \mathbf{c} \\ \text{s.t. } \mathbf{A}_{\text{ineq}} \mathbf{c} &\leq \mathbf{b}_{\text{ineq}} \end{aligned} \quad (1)$$

where  $\mathbf{c} \in \mathbb{R}^N$  is the optimization variable,  $\boldsymbol{\lambda} \in \mathbb{R}^N$  is the cost vector, and  $\mathbf{A}_{\text{ineq}} \in \mathbb{R}^{M \times N}$  and  $\mathbf{b}_{\text{ineq}} \in \mathbb{R}^M$  represent the inequality constraints. Given such a problem, either 1) the inequality constraints are infeasible, in which case,  $\bar{p} = \infty$ ; 2) the problem is unbounded, in which case,  $\bar{p} = -\infty$ ; or 3) the problem is bounded, and the feasible region non-empty, in which case,  $\bar{p}$  is finite. The feasible set is an intersection of halfspaces, which is a convex set known as a polyhedron. One property of LPs is that, if the optimal value is finite, an optimal solution,  $\bar{\mathbf{c}}$ , always occurs at a basic feasible point. A basic feasible point, which is also known as an extreme point, is one at which the residual, which is given by  $\mathbf{b}_{\text{ineq}} - \mathbf{A}_{\text{ineq}} \mathbf{c}$ , is non-negative and is zero for at least  $N$  rows, and the matrix  $\bar{\mathbf{A}}_{\text{ineq}}$  that contains the rows of  $\mathbf{A}_{\text{ineq}}$  with zero residuals is of full rank.

Every LP has a dual formulation, which is given by

$$\begin{aligned} \bar{d} &= \max_{\mathbf{z}} -\mathbf{z}^T \mathbf{b}_{\text{ineq}} \\ \text{s.t. } \mathbf{A}_{\text{ineq}}^T \mathbf{z} + \boldsymbol{\lambda} &= 0 \\ \mathbf{z} &\geq 0 \end{aligned} \quad (2)$$

where  $\mathbf{z} \in \mathbb{R}^M$  is the dual variable. In bounded feasible LPs,  $d \leq p$ , i.e., the objective function of the dual problem is a lower bound for the primal problem. Excepting special cases, the bound is, in fact, tight, and equality occurs only for  $\bar{d} = \bar{p}$ , corresponding to the optimal solutions of the dual and primal problems, respectively.

Active-set methods such as the well-known simplex method [19] are frequently used to solve LPs. These methods jump from one basic feasible point to another that has a lower objective value. Thus, active-set methods are descent methods, and each

iteration has a lower objective value than the previous one. At each iteration, a dual solution is generated by computing  $\bar{\mathbf{z}} = -\bar{\mathbf{A}}_{\text{ineq}}^{-T} \boldsymbol{\lambda}$ , which is a subvector of  $\mathbf{z}$ . The remaining entries of  $\mathbf{z}$  are taken to be zero. If  $\bar{\mathbf{z}} \geq 0$ , then the current iterate is optimal.

In solving LPs using active-set methods, an initial extreme point must be found. In general, this is nontrivial and requires the solution of a special phase I LP. In the event that a point within the feasible polyhedron is known, an extreme point of the polyhedron can be found in a number of ways. One is to move in the direction of  $-\boldsymbol{\lambda}$  until a constraint is encountered. There is now at least one active constraint, and we move in the direction of the projection of  $-\boldsymbol{\lambda}$  on the set of active constraints until more constraints are encountered. This is repeated until the set of active constraints has full rank, at which point an extreme point has been reached.

While there are many different approaches to solve LPs, in this paper, we introduce a novel LP formulation for which an active-set solver is particularly efficient. This is described in Section III-C2.

### III. SAFE TENSION DISTRIBUTIONS

#### A. Definition of the Tension-Distribution Problem

Completely restraining a cable-driven robot requires the existence of a strictly positive right null vector of the structure matrix, i.e.,  $\mathbf{A} \in \mathbb{R}^{n \times m}$  [9]. A necessary condition for the existence of such a null vector is that the number of cables exceeds the number of DOFs, i.e.,  $m > n$ . The vector  $\mathbf{A}$  must also have full rank. Furthermore, in order to deliver a desired wrench,  $\mathbf{w} \in \mathbb{R}^n$ , a set of tensions,  $\mathbf{f} \in \mathbb{R}^m = [T_1 \ \cdots \ T_m]^T$ , must meet the following equality:

$$\mathbf{A}\mathbf{f} = \mathbf{w}. \quad (3)$$

As cables are unable to exert pushing forces, all cable tensions must be positive, and, in general, above some positive lower tension limit  $T_{\min}$ . Additionally, the finite-torque capabilities of system actuators impose an upper limit  $T_{\max}$  on cable tension. Furthermore, the goal of optimization is to minimize some objective function  $g(\mathbf{f})$  subject to these constraints

$$\begin{aligned} \mathbf{f}^* &= \underset{\mathbf{f}}{\operatorname{argmin}} g(\mathbf{f}) \\ \text{s.t. } \mathbf{A}\mathbf{f} &= \mathbf{w} \\ T_{\min} \begin{bmatrix} 1 \\ \vdots \\ 1 \end{bmatrix}_m &\leq \mathbf{f} \leq T_{\max} \begin{bmatrix} 1 \\ \vdots \\ 1 \end{bmatrix}_m. \end{aligned} \quad (4)$$

Previous work has considered both  $g(\mathbf{f}) = \|\mathbf{f}\|_1$  [5] and  $g(\mathbf{f}) = \|\mathbf{f}\|_2$  [15], [17]. In the former case, the optimization becomes an LP. A significant shortcoming of tension distributions resulting from this formulation is that they are prone to discontinuities in which an infinitesimally small change in end-effector position or desired wrench can yield a finite change in tension [15], [16]. The resulting step change in desired tensions can excite high-frequency modes and degrade robot stability. On the other hand, if the objective function  $\|\mathbf{f}\|_2$  is used, then the optimization becomes a QP with linear constraints. Significantly,

the resulting tension distributions are not prone to discontinuous behavior.

Both the LP and QP formulations can be solved by standard convex-optimization methods, because the objective functions are convex over the feasible space, which is also convex. As described in Section II, these methods require the solution of a special phase I problem to find a feasible starting point. In a highly dynamic system, rapid computation of tension distributions is critical for robot performance. Thus, the cost associated with solving a separate phase I problem can dramatically decrease the update rate of the tension control loop, thereby reducing the control bandwidth.

#### B. Previous Work in Safe Tension Distributions

A significant issue associated with previous LP and QP formulations is that the resulting tension-distributions frequently contain cable tensions that are equal to  $T_{\min}$  or  $T_{\max}$ , as is shown in Section IV. These limits represent extreme operating regions. A system that routinely operates at these points will frequently encounter near-slack conditions in the case of operation at lower tension limits and excessively high-torque requirements in the case of operation at upper tension limits. To ameliorate this, Mikelsons *et al.* [16] recently presented a noniterative algorithm that computes “safe” and continuous tension distributions for redundant platforms. The distributions are “safe” in that they lie at the center of gravity (CoG) of the manifold  $\mathcal{P}$  of feasible tension distributions that exert the desired wrench on the end-effector. Thus, they avoid tension limits, which reduces the likelihood of slack conditions.

To compute the CoG of  $\mathcal{P}$ , Mikelsons *et al.* [16] first find all of its vertices. These vertices are intersection points of at least  $r$  of the  $2m$  tension constraints. All possible combinations of  $r$  of the  $2m$  constraints must be considered, and for each combination, the corresponding intersection must be computed. If such an intersection complies with all tension inequalities, then it is a vertex of  $\mathcal{P}$ .

The deterministic, noniterative nature of this algorithm recommends its use for systems in which the force distribution must be computed during each servoloop under real-time constraints. However, the combinatorial nature of considering all combinations of  $r$  out of  $2m$  constraints indicates that this method becomes computationally intractable, even for moderately complex platforms. In a general case, selecting  $r$  out of  $2m$  constraints results in

$$\binom{2m}{r} \quad (5)$$

possible combinations. However, the  $2m$  constraints contain  $m$  pairs of two parallel hyperplanes. Because parallel hyperplanes never intersect, each combination can contain at most one constraint from each pair. For example, if  $m = 3$ ,  $r = 2$ , and the constraints are arranged such that constraints  $2k - 1$  and  $2k$ , where  $k = 1, \dots, m$  are parallel, then the possible combinations are  $\{(1,3) (1,4) (1,5) (1,6) (2,3) (2,4) (2,5) (2,6) (3,5) (3,6) (4,5) (4,6)\}$ , and combinations such as  $\{(1,2) (3,4) (5,6)\}$ , which contain parallel constraints, need not be considered. Thus,

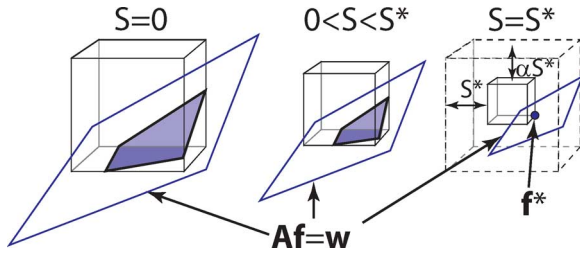


Fig. 1. Constraints in (8) shown to increase  $S$ . The  $m$ -dimensional hypercube represents the tension limits posed by the second constraint in (8). As  $S$  increases, the hypercube shrinks until only one point satisfying  $\mathbf{A}\mathbf{f} = \mathbf{w}$  remains within the hypercube. This point is  $\mathbf{f}^*$ .

selecting  $r$  constraints becomes analogous to selecting  $r$  of the  $m$  pairs and considering every possible combination of these  $r$  pairs. There are

$$\binom{m}{r} \quad (6)$$

ways of selecting  $r$  pairs, and for each such selection, there are  $2^r$  combinations. Thus, the total number of combinations that must be considered in finding all the extreme points  $\mathcal{P}$  is given by

$$2^r \binom{m}{r}. \quad (7)$$

Thus, merely computing the potential vertices of  $\mathcal{P}$  becomes prohibitively burdensome, even for moderately complex systems. For example, in the case of the nine-cable, 6-DOF Wiro 6.3 robot introduced in Section IV, (7) yields 672 possible combinations.

### C. OS Tension Distributions

1) *LP Problem Formulation:* In this section, we present an LP method that computes OS tension distributions by introduction of a slack variable  $S$ . The formulation of this problem is as follows:

$$\hat{S} = \max_{\mathbf{f}, S} S$$

$$\text{s.t. } \mathbf{A}\mathbf{f} = \mathbf{w}$$

$$(T_{\min} + S) \begin{bmatrix} 1 \\ \vdots \\ 1 \end{bmatrix}_m \leq \mathbf{f} \leq (T_{\max} - \alpha S) \begin{bmatrix} 1 \\ \vdots \\ 1 \end{bmatrix}_m \quad (8)$$

for some  $\alpha \geq 0$ , where the optimization variables are the tension vector  $\mathbf{f}$  and the slack variable  $S$ .

The second constraint in (8) represents an  $m$ -dimensional hypercube wherein the upper limits are given by  $T_{\max} - \alpha S$ , and the lower limits are given by  $T_{\min} + S$  (see Fig. 1). The feasible set of tensions consists of the solutions  $\hat{\mathbf{f}}$  to  $\mathbf{A}\mathbf{f} = \mathbf{w}$  that lie within this hypercube. As  $S$  increases, the hypercube shrinks until only one solution of the equality remains within the hypercube. This point is  $\mathbf{f}^*$ . In the case where  $\alpha = 1$ ,  $\mathbf{f}^*$  is the OS operating point, in that it is the solution of the underdetermined linear equality  $\mathbf{A}\mathbf{f} = \mathbf{w}$  that maximizes the minimal element of

the vector

$$\boldsymbol{\epsilon} = \begin{bmatrix} \mathbf{f} - \mathbf{T}_{\min} \\ \mathbf{T}_{\max} - \mathbf{f} \end{bmatrix} \quad (9)$$

where  $\mathbf{T}_{\min}$  and  $\mathbf{T}_{\max}$  are appropriately sized vectors.  $\boldsymbol{\epsilon}$  represents the difference between OS tensions and cable boundaries, and maximizing its minimal element corresponds to maximizing the distance between  $\mathbf{f}^*$  and the closest tension boundary.

Selection of  $\alpha$  allows the user to steer cable tensions toward low- or high-tension regions of operation. If  $\alpha$  is large, then the upper limit decreases faster than the lower limit increases, and  $\mathbf{f}^*$  tends to contain lower tensions. Conversely, if  $\alpha$  is small, then the lower limit increases quickly, and cable tensions tend to increase. We note here that, if  $\hat{S}$  is negative, then there exists no set of tensions that satisfies the conditions of (8), and the tension-distribution problem is infeasible. However, (8) places no constraint on the sign of  $S$ , and the tension distribution that least violates tension limits is computed. Thus, in the event of infeasibility, the OS formulation performs gracefully and yields a meaningful result.

Besides providing OS tension distributions, the slack variable  $S$  enables explicit computation of a starting point that is not only feasible but close to the global optimum as well. The proximity of this starting point to the global optimum results in very fast convergence for active-set methods.

2) *Efficient Computation Methods:* We begin with (3) and partition the structure matrix  $\mathbf{A}$  into two matrices, i.e.,  $\mathbf{B} \in \mathbb{R}^{n \times n}$  and  $\mathbf{H} \in \mathbb{R}^{n \times r}$ , where  $r = m - n$  is the degree of actuation redundancy presented by the robot as

$$\mathbf{A} = [\mathbf{B} \mid \mathbf{H}]. \quad (10)$$

Similarly, we partition the tension vector into two vectors, i.e.,  $\mathbf{f}_1 \in \mathbb{R}^n$  and  $\mathbf{f}_2 \in \mathbb{R}^r$ . Thus

$$\mathbf{A}\mathbf{f} = [\mathbf{B} \mid \mathbf{H}] \begin{bmatrix} \mathbf{f}_1 \\ \mathbf{f}_2 \end{bmatrix} = \mathbf{w}. \quad (11)$$

Solving  $\mathbf{f}_1$  yields

$$\mathbf{f}_1 = \mathbf{B}^{-1}(\mathbf{w} - \mathbf{H}\mathbf{f}_2). \quad (12)$$

Depending on robot configuration, care must be exercised to ensure that  $\mathbf{B}$  is of full rank. During operation in nonsingular regions, the structure matrix  $\mathbf{A}$  is full rank [9], and it is always possible to select  $n$  linearly independent columns by reordering. The method used to select linearly independent columns of  $\mathbf{A}$  may vary depending on platform type. For some robots, a given set of columns will be linearly independent for all end-effector configurations within the workspace. This is true of NIMS-PL, which is introduced in Section IV-A. In this platform, two adjacent cables are never collinear for end-effectors within the workspace, and therefore, any such pair of cables can be selected in generating  $\mathbf{B}$ . If no such special property exists, a QR decomposition of  $\mathbf{A}$  can be used to find linearly independent columns.

We see from (12) that a tension distribution  $\mathbf{f}$  can be completely determined by finding  $\mathbf{f}_2 \in \mathbb{R}^r$ . Using this property, the

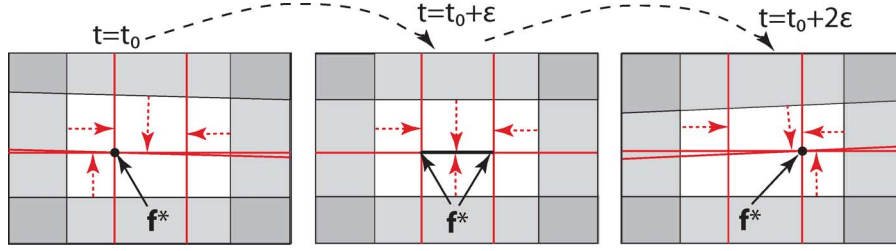


Fig. 2. Step discontinuity in  $\mathbf{f}^*$  caused by a small change in the feasible polyhedron described by (13). Red arrows indicate movement of constraining hyperplanes to increase  $S$ , and red lines show the hyperplanes at  $S^*$ . At time  $t = t_0$ , there is a unique  $\mathbf{f}^*$ , but at  $t = t_0 + \epsilon$ , the polyhedron becomes a rectangle, and  $\mathbf{f}^*$  becomes nonunique. At time  $t = t_0 + 2\epsilon$ , the solution again becomes unique but has undergone a discontinuity.

optimization in (8) can be expressed in the following LP form:

$$\begin{aligned}
 \mathbf{y}^* &= \underset{\mathbf{y}}{\operatorname{argmin}} \mathbf{d}^T \mathbf{y} \\
 \text{s.t. } \mathbf{A}_{\text{LP}} \mathbf{y} &\leq \mathbf{b}_{\text{LP}}, \quad \text{where} \\
 \mathbf{y} &= \begin{bmatrix} \mathbf{f}_2 \\ S \end{bmatrix}, \quad \mathbf{d} = [\mathbf{0}_m^T \mid -1]^T \\
 \mathbf{A}_{\text{LP}} &= \left[ \begin{array}{c|c} -\mathbf{I}_r & \mathbf{1}_r \\ \mathbf{B}^{-1} \mathbf{H} & \mathbf{1}_n \\ \mathbf{I}_r & \alpha \mathbf{1}_r \\ -\mathbf{B}^{-1} \mathbf{H} & \alpha \mathbf{1}_n \end{array} \right] = [\mathbf{A}_{\text{LP}_1} \mid \mathbf{a}_{\text{LP}_2}], \quad \text{and} \\
 \mathbf{b}_{\text{LP}} &= \begin{bmatrix} -\mathbf{T}_{\min} \\ -\mathbf{T}_{\min} + \mathbf{B}^{-1} \mathbf{w} \\ \mathbf{T}_{\max} \\ \mathbf{T}_{\max} - \mathbf{B}^{-1} \mathbf{w} \end{bmatrix}. \quad (13)
 \end{aligned}$$

Because (13) is solved during each iteration of the servoloop, we expect the optimal solution found during the  $M - 1$ th loop, i.e.,  $\mathbf{y}_{M-1}^* = [\mathbf{f}_{2M-1}^* \mid S_{M-1}^*]^T$ , to be close to  $\mathbf{y}_M^*$ , as only one servocycle has elapsed. We begin by checking if the corresponding set of active constraints, i.e.,  $\bar{\mathbf{A}}_{\text{LP}_{M-1}}$ , still yields an optimal result. As described in Section II, this is accomplished by computing a dual  $\mathbf{z}$  and checking whether  $\mathbf{z} \geq 0$ . If this is the case, then the optimal solution to (13) has been found. If  $\mathbf{z}$  contains negative elements, but the point  $\mathbf{y}_{\text{new}} = \bar{\mathbf{A}}_{\text{LP}_{M-1}}^{-1} \bar{\mathbf{b}}_{\text{LP}_{M-1}}$  still represents an extreme point for (13), then we begin the simplex method with this point as the starting iterate.

If  $\mathbf{y}_{\text{new}}$  is not feasible, a feasible and near-optimal starting point can be explicitly found by relaxing the slack variable  $S$  until feasibility is achieved. In doing so, we reduce  $S$  just enough to make the starting point feasible. The largest  $S$  for which  $\mathbf{f}_{2M-1}$  is feasible for the  $M$ th servoloop can be found explicitly as follows:

$$S_{\max_M} = \min((\mathbf{b}_{\text{LP}} - \mathbf{A}_{\text{LP}_1} \mathbf{f}_{2M-1}) ./ \mathbf{a}_{\text{LP}_2}) \quad (14)$$

where we use the “./” notation to indicate component-wise division. In other words,  $S_{\max_M}$  is the largest value of  $S$  for which

$$\mathbf{b}_{\text{LP}} - [\mathbf{A}_{\text{LP}_1} \mid \mathbf{a}_{\text{LP}_2}] \begin{bmatrix} \mathbf{f}_{2M-1} \\ S \end{bmatrix} \geq 0.$$

It should be noted that  $S_{\max_M}$  can be negative. However, this still corresponds to a feasible starting point in (8), which places no explicit constraint on the sign of  $S$ . However, if the subsequent optimization does not generate a nonnegative value of  $S^*$ , then the problem is infeasible.

The resulting vector  $\mathbf{y}_{0M} = [\mathbf{f}_{2M-1} \mid S_{\max_M}]^T$  is now a feasible starting point from which an extreme point can be found, as described in Section II. Once an extreme point has been found, the well-known simplex method is used to find the global optimum.

We expect agreement between the starting iterate and the optimal point to improve as the sampling rate increases. As is shown in Section V, the proximity of the starting point to the optimal value results in fast convergence to the global optimum.

3) *On the Continuity of OS Tension Distributions:* A simple example shows that OS tensions can undergo step discontinuities in response to infinitesimally small changes in the shape of the set of feasible tensions. This is shown in Fig. 2. These discontinuities occur when the set of active constraints in the solution to (13) becomes singular. However, we have not witnessed such behavior in any of our simulations or experiments on several different cable-driven platforms. Continuity for other platforms can be ensured by offline prechecking or online supervision to stop the system in case of discontinuous tension distributions.

#### IV. STATIC TENSION-DISTRIBUTION SIMULATIONS

In this section, we present results showing the distribution of OS tensions for two simulated robotic systems. The first system considered is a four-cable-driven, 2-DOF system known as NIMS-PL [11]. The second is a nine-cable-driven, 6-DOF robot known as WiRo-6.3 [20].

##### A. NIMS-PL

NIMS-PL is a four-cable-driven, 2-DOF robot intended for actuated-sensing applications in aquatic environments [11]. A schematic diagram is shown in Fig. 3, and a kinematic representation is shown in Fig. 4. For this system, the  $i$ th column of the structure matrix  $\mathbf{A}_{\text{NIMS}} \in \mathbb{R}^{2 \times 4}$  is given by  $\mathbf{a}_i = \mathbf{p}_i - \mathbf{x} / \|\mathbf{p}_i - \mathbf{x}\|$ , which is the unit vector directed from the end-effector  $\mathbf{x}$  toward the  $i$ th cable origin  $\mathbf{p}_i$ , i.e.,

$$\mathbf{A}_{\text{NIMS}} = [\mathbf{a}_1 \quad \mathbf{a}_2 \quad \mathbf{a}_3 \quad \mathbf{a}_4]. \quad (15)$$

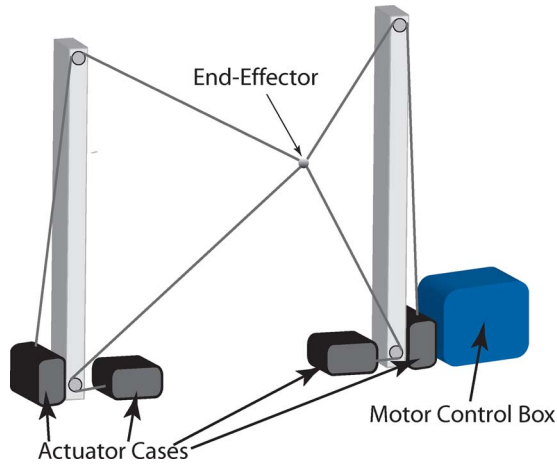


Fig. 3. Schematic diagram of NIMS-PL showing actuator cases, the controller case, and point-mass end-effector.

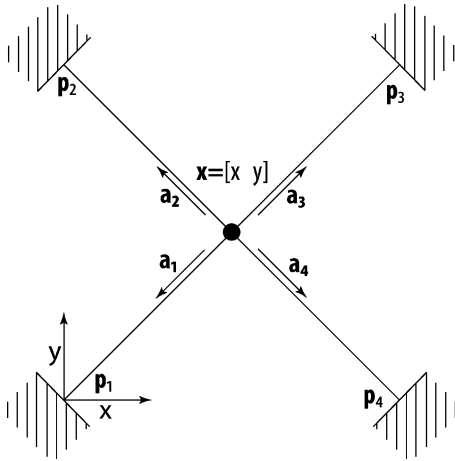


Fig. 4. Kinematic diagram of a NIMS-PL configuration showing cable origins  $\mathbf{p}_i$ , end-effector position  $\mathbf{x} = [x \ y]^T$ , and unit vectors  $\mathbf{a}_i$ , in the directions of corresponding cables.

For our simulations, we consider a square horizontal workspace with dimension  $1 \text{ m} \times 1 \text{ m}$  in which a 5-kg point mass supported by a frictionless surface is actuated. The tension limits are given by  $T_{\min} = 10 \text{ N}$  and  $T_{\max} = 100 \text{ N}$ .

### B. WiRo-6.3

The second cable-driven robotic system considered in our simulations is WiRo-6.3 [20], a 6-DOF, nine-cable robot. A schematic diagram is shown in Fig. 5. Ferraresi *et al.* [20] describe several advantages of WiRo6.3, including a large feasible workspace and the existence of closed-form solutions to inverse- and forward-kinematic routines. The structure matrix  $\mathbf{A}_{\text{WiRo}} \in \mathbb{R}^{6 \times 9}$  can be computed as in, for example, [16]. Following the definitions in Fig. 5, in our simulations, we take  $r_A = r_B = h = 1.00 \text{ m}$ , and the end-effector is a thin 5 kg disc with radius 0.2 m. The tension limits are given by  $T_{\min} = 10 \text{ N}$  and  $T_{\max} = 100 \text{ N}$ .

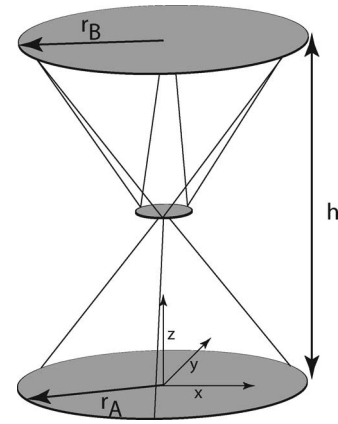


Fig. 5. Schematic of a WiRo-6.3 configuration.  $r_B$  and  $r_A$  are the distances from the center of the top and bottom frames to the cable insertion points, and  $h$  is the distance between these planes.

### C. Static Tension Results

In order to demonstrate the effect of OS tension distributions, we randomly select a large number of feasible static configurations for each system and compute the corresponding tension distributions. To demonstrate the effect of varying  $\alpha$  on the resulting tension distributions, we consider  $\alpha = 0.5, 1$ , and  $2$ .

1) *Static NIMS-PL Results:* For NIMS-PL, we consider 1000 randomly selected static configurations, with 4000 corresponding tensions. The results are shown in histogram form in Fig. 6 compared with the  $\mathbf{L}^1$ -minimal solution. It is readily apparent that the  $\mathbf{L}^1$  tension distributions frequently result in operating points on the lower tension limit. In fact, for static NIMS-PL configurations, two of the four cables are always on the lower tension limit. For the OS distributions, it is evident that the tension limits are successfully avoided. Furthermore, varying  $\alpha$  has the intended effect on the tension distributions, as the  $\alpha = 0.5$  plot shows a higher concentration of cable tensions in the upper tension region, while the  $\alpha = 2$  plot shows more cables operating under lower tensions. This is further evident in the average cable tensions, which are given in Table I.

In order to demonstrate the ability of OS tension distributions to avoid operation at boundary conditions, we plot the cumulative distribution function (CDF) of the distance of cable tensions from the closest boundary condition in Fig. 7. The CDFs for  $\alpha = 0.5, 1$ , and  $2$  are plotted and compared against that of the  $\mathbf{L}^1$ -minimal tension distribution. It is evident that the OS tension distributions are very effective in avoiding boundary conditions. Furthermore, we see that  $\alpha$  has little effect on the proximity of cable tensions to boundary conditions.

### D. Static WiRo-6.3 Results

For WiRo-6.3, we again consider 1000 randomly selected static configurations with 9000 corresponding tensions. The results are shown in histogram form in Fig. 8, compared with the  $\mathbf{L}^1$ -minimal solution. Once again, the  $\mathbf{L}^1$  tension distributions frequently result in operating points on the lower tension limit. Of the 9000 cable tensions considered, 2996 lie on the lower tension boundary, while four lie on the upper limit. For OS



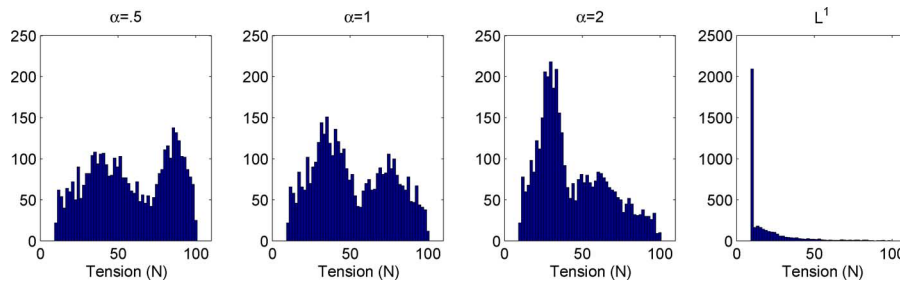


Fig. 6. Histograms of tension distributions for NIMS-PL with  $\alpha = 0.5, 1,$  and  $2,$  as compared with the  $L^1$ -minimal solution.

TABLE I  
MEAN CABLE TENSIONS FOR STATIC NIMS-PL CONFIGURATIONS

	$\alpha = .5$	$\alpha = 1$	$\alpha = 2$	$L^1$
Avg T (N)	57.4	51.6	44.1	19.3

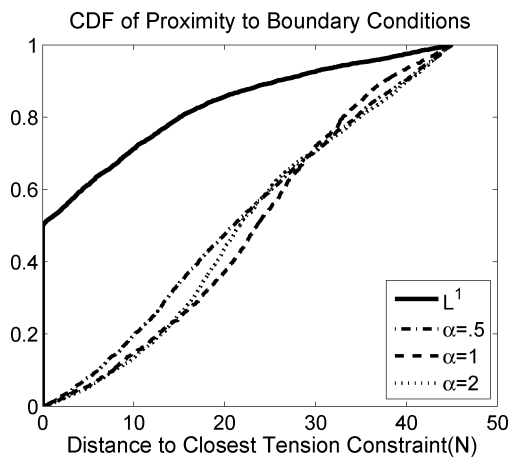


Fig. 7. CDF of the proximity of cable tensions to boundary conditions on NIMS-PL for  $\alpha = 0.5, 1,$  and  $2,$  as compared with  $L^1$ -minimal distributions.

distributions, boundary conditions are once again successfully avoided, although the effect of varying  $\alpha$  is more subtle than in the NIMS-PL case. While increasing  $\alpha$  does noticeably shift tensions into lower regions, the effect is much less dramatic for this system. The average cable tensions, which are given in Table II, also indicate a smaller shift in mean tension than in the NIMS-PL case. This is caused by the increased number of tension constraints imposed by the larger number of cables used to drive the end-effector in the WiRo system. As the number of cables increases, the flexibility in selecting  $\mathbf{f}$  tends to decrease, and the effects of varying  $\alpha$  become less dramatic.

We plot the CDF of the distance of cable tensions from the closest boundary condition in Fig. 9. The CDFs for  $\alpha = 0.5, 1,$  and  $2$  are shown with that of the  $L^1$  tension distribution. Again, it is evident that the OS tension distributions are effective in avoiding boundary conditions. The difference as compared with  $L^1$  tension distributions is less exaggerated than in the NIMS-PL case because of the increased number of tension constraints posed by the larger number of wires in the WiRo 6.3 system. Once again, selection of  $\alpha$  has little effect on proximity

to boundary conditions, as the traces used to vary  $\alpha$  are nearly indistinguishable in Fig. 9.

It is clear that OS tension distributions successfully avoid cable tension limits for the values of  $\alpha$  considered in these simulations. However, avoiding frequent operation near the lower tension limit incurs the cost of somewhat increased operation near upper tension limits. If operation near such limits is particularly unsafe for some application, then users might select larger values for  $\alpha$ . In this case, operation near upper tension limits is significantly reduced, as lower tensions are favored. Thus, through proper selection of  $\alpha$ , a wide range of desired performance characteristics can be addressed.

## V. DYNAMIC TENSION-DISTRIBUTION SIMULATIONS

While the results presented in Section IV show the effectiveness of OS tension distributions in avoiding tension limits, the configurations considered are static, and therefore, nothing can be said about computational efficiency. In order to enable such analysis, we simulated the execution of highly dynamic trajectories for both NIMS-PL and WiRo-6.3 for  $\alpha = 1$  and for servofrequencies ranging from 5 to 50 Hz. We show that, even for the complex WiRo-6.3 system with a servorate of 50 Hz, which exceeds the bandwidth of typical tension-control systems, the worst-case computational burden of computing OS tension distributions consumes only a small fraction of the processing power of commercially available embedded processors.

It should be noted that these simulations consider end-effector dynamics but ignore other dynamic effects, such as those introduced by cables and actuator systems. Including these effects would influence the desired output wrench  $\mathbf{w}$  and may slightly increase the computational burden required in the optimization. However, the presented results indicate that the computational burden associated with computing OS tension distributions is very small and that the optimization would still be manageable despite moderate increases in complexity.

### A. NIMS-PL Dynamic Results

In order to evaluate the computational efficiency of our LP solver for NIMS-PL, we simulated the execution of a highly dynamic trajectory on the same NIMS-PL configuration considered in the previous section. The trajectory considered is a triangle with start and end points given in Table III. In this simulation, the maximum velocity is 2 m/s, and the maximum

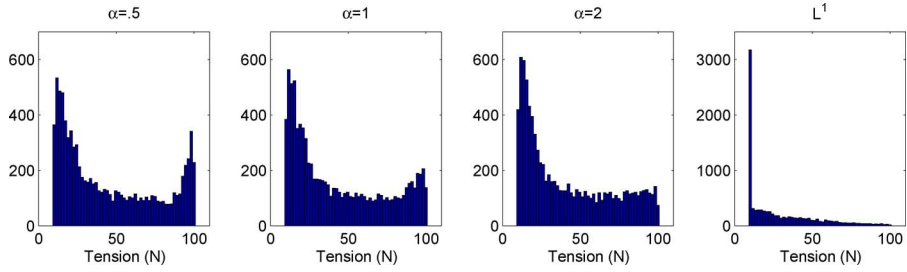


Fig. 8. Histograms of tension distributions for WiRo-6.3 with  $\alpha = 0.5, 1,$  and  $2,$  as compared with the  $L^1$ -minimal solution.

TABLE II  
MEAN CABLE TENSIONS FOR STATIC WiRO-6.3 CONFIGURATIONS

	$\alpha = .5$	$\alpha = 1$	$\alpha = 2$	$L^1$
Avg T (N)	45.5	44.0	41.8	28.6

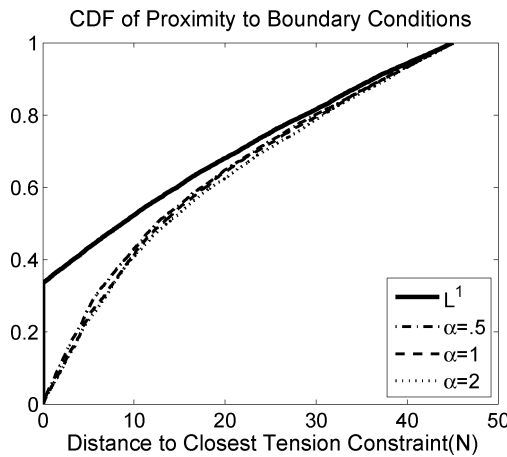


Fig. 9. CDF of the proximity of cable tensions to boundary conditions on WiRo-6.3 for  $\alpha = 0.5, 1,$  and  $2,$  as compared with  $L^1$ -minimal distributions.

TABLE III  
START AND END POINTS FOR TRIANGULAR TRAJECTORY EXECUTED BY NIMS-PL

Path Number	1	2	3
Start Point [x, y](m)	[.5, .2]	[.3, .8]	[.8, .7]
End Point [x, y](m)	[.3, .8]	[.8, .7]	[.5, .2]

acceleration is  $10 \text{ m/s}^2$ . Furthermore, an s-curve trajectory is used, wherein the acceleration profile is continuous and rises to its maximum value in  $0.02 \text{ s}$ . The duration of the entire triangular trajectory, shown in Fig. 10, is  $1.52 \text{ s}$ .

The mean number of active-set iterations required for convergence is shown against servofrequency in Fig. 11. It is apparent that the number of iterations per servoloop decreases significantly as the servouppdate rate increases. This is in accordance with expectations, as the starting point for each iteration, which is given by the optimal value from the previous iteration, becomes closer to the new optimal value as the sample rate increases.

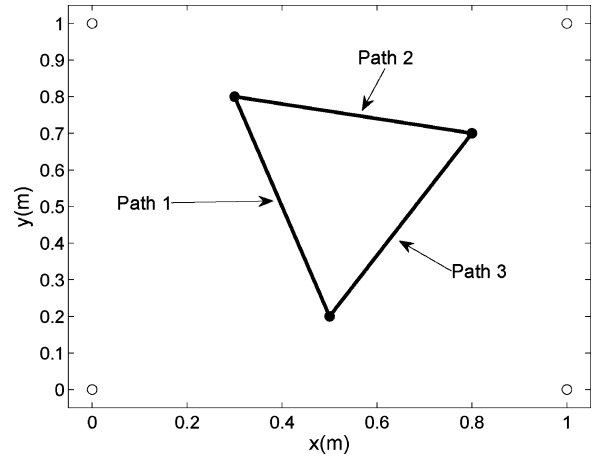


Fig. 10. Simulated NIMS-PL trajectory.

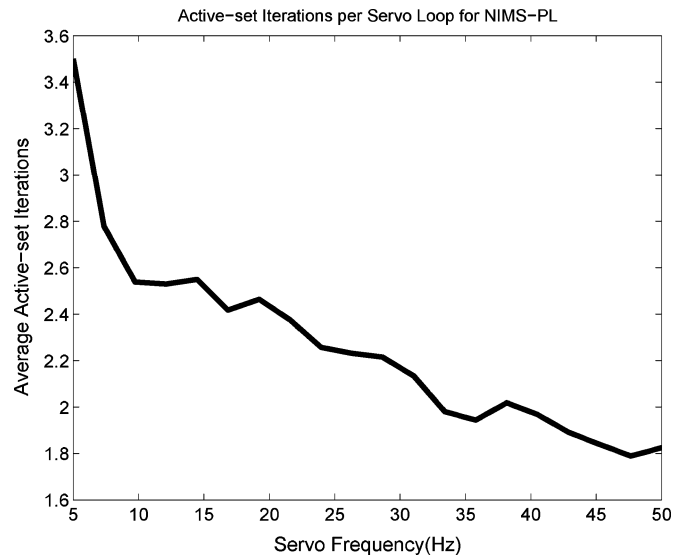


Fig. 11. Active-set iterations per servoloop shown against servofrequency.

Because robotic systems are subject to real-time constraints, it is critical that the tension optimization be entirely completed during each servoloop. Thus, worst-case performance must not be exceedingly poor. In this simulation, the largest number of iterations required for convergence was 5. The greatest computational burden required of the CPU was approximately 580



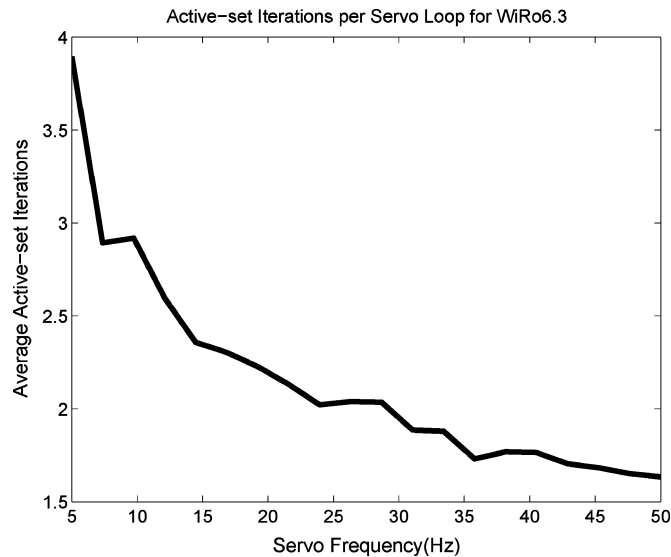


Fig. 12. Active-set iterations per servoloop shown against servofrequency.

floating-point operations (FLOPs) at an update rate of 48 Hz, which corresponds roughly to 27 kFLOPs/s. This represents a very small fraction of the computational power of modern embedded processors. The average computational burden at 50 Hz was 9.7 kFLOPs/s.

### B. WiRo-6.3 Dynamic Results

In order to evaluate the computational efficiency of computing OS solutions for a more complex system, we simulated the execution of a highly dynamic trajectory on the same WiRo-6.3 configuration considered in the previous section. We define the position vector  $\mathbf{x} = [x \ y \ z \ \theta_x \ \theta_y \ \theta_z]^T$ , where the units of the translational DOFs are meters, and the units of the rotational DOFs are radians. The trajectory starts and ends at  $\mathbf{x} = [0 \ 0 \ 0.2 \ 0 \ 0 \ 0.35]^T$ , and consists of the following five parts:

- 1) move in a straight line to  $\mathbf{x} = [0 \ 0 \ .8 \ 0 \ 0 \ -.35]^T$ ;
- 2) move in a straight line to  $\mathbf{x} = [0 \ 0 \ .6 \ 0 \ 0 \ 0]^T$ ;
- 3) move in a straight line to  $\mathbf{x} = [.35 \ 0 \ .6 \ 0 \ 0 \ 0]^T$ ;
- 4) execute a circle with radius 0.35 m about the  $z$ -axis;
- 5) return to the starting point.

For all trajectory segments, the maximum velocity is 1.5 m/s, and the maximum acceleration is 10 m/s<sup>2</sup>. Again, an s-curve trajectory is used, wherein the acceleration profile is continuous and rises to its maximum value in  $t_a = 0.05$  s. The duration of the entire trajectory is 4.02 s.

The mean number of active-set iterations required for convergence is shown against servofrequency in Fig. 12. Again, the number of iterations per servoloop decreases significantly as the servoupdate rate increases.

In this simulation, the highest computational burden during a single servoloop was eight active-set iterations with a servorate of 48 Hz, which corresponds to approximately 110 kFLOPs/s. The average computational burden at 50 Hz was 24 kFLOPs/s. Again, this represents a small fraction of the computational

power of commercially available embedded processors. Thus, we see that our method of computing OS tensions is sufficiently fast for a 6-DOF, nine-cable robot executing a highly dynamic trajectory, even with an update rate that far exceeds the bandwidth of typical tension-control systems.

In order to compare our algorithm to that of the noniterative method presented in [16], we again consider that, for a 6-DOF, nine-cable robot, (7) yields that 672 intersections of hyperplanes must be computed. This requires solving 672 sets of linear equations in  $\mathbb{R}^3$ . If Gaussian elimination is used, computing one of these solutions requires 28 FLOPs, and evaluating whether it is feasible requires an additional 90 FLOPs. Thus, approximately 80 kFLOPs are required to find the vertices of the feasible polyhedron  $\mathcal{P}$ . If the servoupdate rate is 50 Hz, then 4 MFLOPs/s are required merely to compute the possible extreme points. Thus, we see that the computational burden presented in finding the extreme points of  $\mathcal{P}$  in the noniterative method of [16] is at least 36 times greater than the worst-case complexity of our algorithm and at least 165 times greater than its average complexity.

## VI. EXPERIMENTAL RESULTS

In order to evaluate the performance of OS tension distributions on an actual physical system, we implemented an OS tension solver on an actual NIMS-PL system, which was configured in a square with side length 1.264 m. For these trials,  $T_{\min} = 20$  N, and  $T_{\max} = 100$  N. Cable tensions were monitored while a circular trajectory centered at 0.632 m with radius 0.35 m was executed at a speed of 0.55 m/s. We consider  $\alpha = 0.5, 1$ , and 2, as well as the  $L^1$ -minimal tension distribution. For these trials, tension distributions were computed at 17.75 Hz on an 80-MHz DSP56300 embedded chip. It should be noted that this CPU can operate at frequencies up to 240 MHz, thereby increasing computational bandwidth and the rate at which tension distributions are computed. Furthermore, modern DSPs are available that vastly outperform our current CPU, and therefore, very high update rates are readily achievable.

No tension discontinuities were observed during the execution of the trajectories. Histograms of the resulting tensions are shown in Fig. 13. We do not expect exact agreement with Fig. 6 because we now consider only points along the experimental trajectory, while in the previous case, we considered a large number of randomly selected points. We observe that increasing  $\alpha$  does noticeably decrease tensions. This is further evident in the mean cable tensions given in Table IV.

It is apparent from Fig. 13 that all tension distributions experience occasional violations of constraints caused by dynamic effects and imperfect tension control. This underscores the importance of maximizing the distance between cable tensions and their imposed limits. For the OS distributions, violations of tension limits are rare, while for the  $L^1$ -minimal distributions, they occur quite frequently. The CDF of the distance of cable tensions from the closest boundary condition is shown in Fig. 14. We see that the use of OS cable tensions dramatically reduces the occurrence of near-slack operating conditions and violation of tension limits.

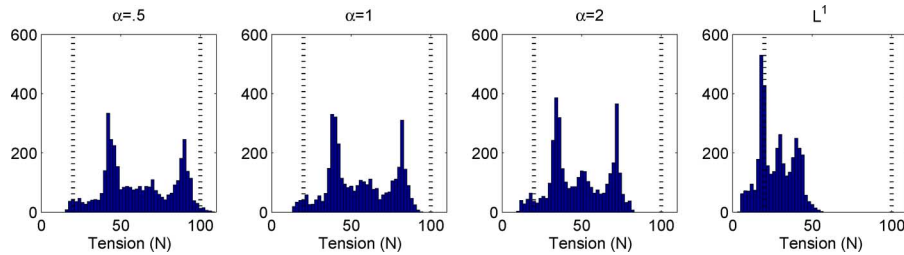


Fig. 13. Histograms of experimental tension distributions for NIMS-PL with  $\alpha = 0.5, 1,$  and  $2,$  as compared with the  $L^1$ -minimal solution. The dotted vertical lines indicate tension limits.

TABLE IV  
MEAN CABLE TENSIONS FOR EXPERIMENTAL EXECUTION OF A CIRCULAR TRAJECTORY ON NIMS-PL

	$\alpha = .5$	$\alpha = 1$	$\alpha = 2$	$L^1$
Avg T (N)	61.0	55.2	48.2	27.4

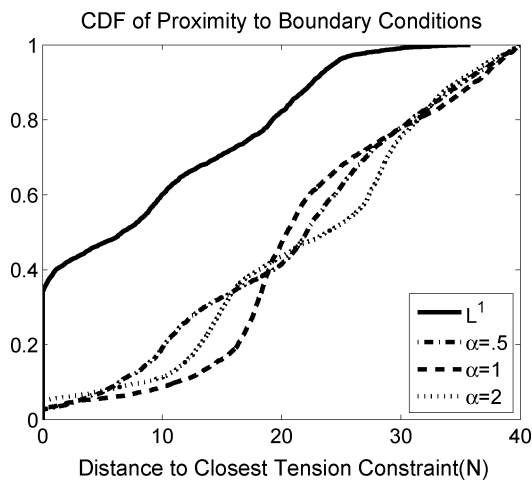


Fig. 14. CDF of the proximity of cable tensions to boundary conditions during performance of experimental trajectory on the physical NIMS-PL system for  $\alpha = 0.5, 1,$  and  $2,$  as compared with  $L^1$ -minimal distributions.

## VII. CONCLUSION

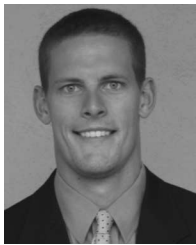
In this paper, we have presented a novel LP formulation that generates OS tension distributions for cable-driven robotic systems. We have shown that introduction of a slack variable enables rapid generation of a feasible starting point from the solution of the previous servoloop. Furthermore, the proximity of this starting point to the global optimum results in rapid convergence to the optimal operating point and, therefore, in a highly efficient computation process. In order to demonstrate the extensibility of our algorithm to platforms with varying DOFs and actuation redundancy, we have considered both a four-cable, 2-DOF system and a nine-cable, 6-DOF system. For both of these platforms, we have presented static tension-distribution simulations that illustrate the ability of our algorithm to avoid near-slack operating conditions. Furthermore, these simulations demonstrate the ability of our LP formulation to favor high- or low-tension configurations, depending on user preference. We have also simulated the execution of highly dynamic trajectories on both robotic platforms to demonstrate the high efficiency of

computing OS tension distributions. We have shown that, for a complex, nine-cable, 6-DOF robot executing a highly dynamic trajectory, our algorithm is sufficiently fast for operation at servoupdate rates far beyond the control bandwidth of typical tension-control systems. In order to evaluate our algorithms on a real robotic system, we implemented them on NIMS-PL, a four-cable 2-DOF robot and executed a circular trajectory. The resulting tension distributions avoided near-slack operating conditions and demonstrated continuous behavior.

## REFERENCES

- [1] P. Bosscher, A. Riechel, and I. Ebert-Uphoff, "Wrench-feasible workspace generation for cable-driven robots," *IEEE Trans. Robot.*, vol. 22, no. 5, pp. 890–902, Oct. 2006.
- [2] M. Gouttefarde and C. Gosselin, "Analysis of the wrench-closure workspace of planar parallel cable-driven mechanisms," *IEEE Trans. Robot.*, vol. 22, no. 3, pp. 434–445, Jun. 2006.
- [3] E. Stump and V. Kumar, "Workspaces of cable-actuated parallel manipulators," *J. Mech. Des.*, vol. 128, no. 1, pp. 159–167, 2006.
- [4] S. Oh and S. Agrawal, "Cable suspended planar robots with redundant cables: Controllers with positive inputs," *IEEE Trans. Robot.*, vol. 21, no. 3, pp. 457–464, Jun. 2005.
- [5] S. Fang, D. Franitza, M. Torlo, F. Bekes, and M. Hiller, "Motion control of a tendon-based parallel manipulator using optimal tension distribution," *IEEE/ASME Trans. Mechatron.*, vol. 9, no. 3, pp. 561–568, Sep. 2004.
- [6] H. Kino, T. Yahiro, F. Takemura, and T. Morizono, "Robust PD control using adaptive compensation for completely restrained parallel-wire driven robots: Translational systems using the minimum number of wires under zero-gravity condition," *IEEE Trans. Robot.*, vol. 23, no. 4, pp. 803–812, Aug. 2007.
- [7] K. Maeda, S. Tadokoro, T. Takamori, M. Hiller, and R. Verhoeven, "On design of a redundant wire-driven parallel robot warp manipulator," in *Proc. Int. Conf. Robot. Autom.*, May 1999, pp. 895–900.
- [8] S. Kawamura, W. Choe, S. Tanaka, and S. Pandian, "Development of an ultrahigh speed robot falcon using wire drive system," in *Proc. IEEE Int. Conf. Robot. Autom.*, 1995, pp. 215–220.
- [9] R. G. Roberts, T. Graham, and T. Lippit, "On the inverse kinematics, statics, and fault tolerance of cable-suspended robots," *J. Robot. Syst.*, vol. 15, no. 10, pp. 581–597, 1998.
- [10] T. Bruckmann, A. Pott, and M. Hiller, "Calculating force distributions for redundantly actuated tendon-based stewart platforms," in *Advances in Robot Kinematics*. New York: Springer-Verlag, 2006, ch. 6, pp. 403–412.
- [11] P. H. Borgstrom, B. L. Jordan, B. J. Borgstrom, M. J. Stealey, G. S. Sukhatme, M. A. Batalin, and W. J. Kaiser, "NIMS-PL: A cable-driven robot with self-calibration capabilities," *IEEE Trans. Robot.*, vol. 25, no. 5, pp. 1005–1015, Oct. 2009.
- [12] W.-J. Shiang, D. Cannon, and J. Gorman, "Dynamic analysis of the cable array robotic crane," in *Proc. IEEE Int. Conf. Robot. Autom.*, 1999, vol. 4, pp. 2495–2500.
- [13] W.-J. Shiang, D. Cannon, and J. Gorman, "Optimal force distribution applied to a robotic crane with flexible cables," in *Proc. IEEE Int. Conf. Robot. Autom.*, 2000, vol. 2, pp. 1948–1954.
- [14] C. Pham, G. Yang, and S. Yeo, "Dynamic analysis of cable-driven parallel mechanisms," in *Proc. IEEE/ASME Int. Conf. Adv. Intell. Mechatron.*, Jul. 24–28, 2005, pp. 612–617.

- [15] P. H. Borgstrom, N. P. Borgstrom, M. J. Stealey, B. Jordan, G. Sukhatme, M. Batalin, and W. Kaiser, "Design and implementation of NIMS3D, a three-dimensional cabled robot for actuated sensing applications," *IEEE Trans. Robot.*, vol. 25, no. 2, pp. 325–339, Apr. 2009.
- [16] L. Mikelsons, T. Bruckmann, M. Hiller, and D. Schramm, "A real-time capable force calculation algorithm for redundant tendon-based parallel manipulators," in *Proc. IEEE Int. Conf. Robot. Autom.*, May 2008, pp. 3869–3874.
- [17] M. Hassan and A. Khajepour, "Optimization of actuator forces in cable-based parallel manipulators using convex analysis," *IEEE Trans. Robot.*, vol. 24, no. 3, pp. 736–740, Jun. 2008.
- [18] D. Bertsimas and J. Tsitsiklis, *Introduction to Linear Programming*. Belmont, MA: Athena Scientific, 1997.
- [19] G. Dantzig, A. Orden, and P. Wolfe, "Generalized simplex method for minimizing a linear form under linear inequality constraints," *Pacific J. Math.*, vol. 5, no. 2, pp. 183–195, 1955.
- [20] C. Ferraresi, M. Paoloni, S. Pastorelli, and F. Pescarmona, "A new 6-dof parallel robotic structure actuated by wires: The wiro-6.3," *J. Robot. Syst.*, vol. 21, no. 11, pp. 581–595, 2004.



**Per Henrik Borgstrom** received the B.S., M.S., and Ph.D. degrees in electrical engineering from the University of California, Los Angeles, in 2005, 2007, and 2009, respectively.

He is currently engaged in post-doctoral research at the University of Southern California, Los Angeles. His interests include cable-driven parallel manipulators, environmental robotics, and optimization.



**Brett L. Jordan** received the B.S. and M.S. degrees in mechanical engineering from the University of California, Los Angeles (UCLA), in 2006 and 2008, respectively.

He is currently working as a Staff Research Engineer with UCLA, where he is involved in mechanical design and product development.



**Gaurav S. Sukhatme** (S'94–M'97–SM'05) received the M.S. and Ph.D. degrees in computer science from the University of Southern California (USC), Los Angeles.

He is currently a Professor of computer science (joint appointment with electrical engineering) with USC, where he is also the Co-Director of the USC Robotics Research Laboratory and the Director of the USC Robotic Embedded Systems Laboratory, which he founded in 2000. His research interests include multirobot systems, sensor/actuator networks, and

robotic sensor networks. He has authored or coauthored numerous papers in these and related areas.

Prof. Sukhatme was the Principal Investigator (PI) of several National Science Foundation (NSF), Defense Advanced Research Projects Agency, and National Aeronautics and Space Administration grants. He is a Co-PI of the Center for Embedded Networked Sensing and the NSF Science and Technology Center. He is a member of the American Association for Artificial Intelligence and the Association for Computing Machinery. He is one of the Founders of the Robotics: Science and Systems Conference. He is the Program Chair of the 2008 IEEE International Conference on Robotics and Automation and the Editor-in-Chief of *Autonomous Robots*. He has served as an Associate Editor for the IEEE TRANSACTIONS ON ROBOTICS and the IEEE TRANSACTIONS ON MOBILE COMPUTING and is a member of the Editorial Board of the *IEEE Pervasive Computing*. He has received the NSF CAREER Award and the Okawa Foundation Research Award.



**Maxim A. Batalin** (S'03–M'05) received the M.S. and Ph.D. degrees in computer science from the University of Southern California, Los Angeles, in 2002 and 2005, respectively.

In 2005, he joined the Wireless Health Program in the Actuated, Sensing, Coordinated, and Embedded Networked Technologies Laboratory, University of California at Los Angeles (UCLA), where, among other projects, he managed the development of the first-of-its-kind incremental diagnosis method for biomedical applications that allows accurate patient-state identification with minimum sensor usage. He is currently a Researcher with the Center for Embedded Networked Sensing. He has been engaged in the research, design, and implementation of systems in areas of robotics, sensors, general biomedical computing, and system integration, UCLA. He has also managed the development of the first end-to-end wireless health monitoring system, i.e., medical embedded devices for individual care (MEDIC), which offers a wireless, wearable architecture for biomedical data acquisition, local processing, and transmittal to a remote enterprise server. He is the author or coauthor of more than 35 conference and journal publications in the areas of wireless health, mobile robotics, sensor networking, actuated sensor systems, biomedical systems, environmental sampling, etc. He also has expertise in the development of software systems for mobile wireless platforms.

Dr. Batalin is a member of Sigma Xi.



**William J. Kaiser** (SM'96) received the Ph.D. degree in solid-state physics from Wayne State University, Detroit, MI, in 1984.

From 1977 to 1986, he was a member of Ford Motor Corporation Research Staff, where he was engaged in the development of automotive sensor and embedded system technology that resulted in large-volume commercial sensor production. He also developed the first spectroscopies directed to microelectronics systems based on scanning tunneling microscopy. From 1986 through 1994, he was with the Jet Propulsion Laboratory, Pasadena, CA, where he initiated the National Aeronautics and Space Administration Microinstrument Program for distributed sensing. In 1994, he joined the faculty of the Electrical Engineering Department, University of California at Los Angeles (UCLA), where he initiated the first Wireless-Networked Microsensor Programs with a vision of linking the Internet to the physical world through distributed monitoring, which includes the topics of low-power embedded computing for wireless-networked sensing, biomedical-embedded computing, robotic sensor systems for environmental monitoring, and distributed-sensing for energy and water-resource management. From 1996 through 2000, he was the Chairman of the Department of Electrical Engineering at UCLA. He has over 170 publications and holds 23 patents.

Dr. Kaiser received the Peter Mark Award of the American Vacuum Society, the National Aeronautics and Space Administration Medal for Exceptional Scientific Achievement, the Arch Colwell Best Paper Award of the Society of Automotive Engineers, the Best Paper Award at BodyNets 2008, two R&D 100 Awards, the Allied Signal Faculty Research Award, the Brian P. Copenhaver Award for Innovation in Teaching with Technology, and the UCLA Gold Shield Faculty Award.